• **Title.**

Cost-effective smartphone-based reconfigurable electrochemical instrument for alcohol determination in whole blood samples

• **Author names and affiliations.**

Joan Aymerich[a] <joan.aymerich@imb-cnm.csic.es>, Augusto Márquez[a] <Augusto.Marquez@imb-cnm.csic.es>, Lluís Terés[a] <lluis.teres@imb-cnm.csic.es>, Xavier Muñoz-Berbel[a] <Xavier.Munoz@imb-cnm.csic.es>, Cecilia Jiménez[a] <cecilia.jimenez@imb-cnm.csic.es>, Carlos Domínguez[a] <carlos.dominguez@imb-cnm.csic.es>, Francesc Serra-Graells[a], <paco.serra@imb-cnm.csic.es>, Michele Dei[a] <michele.dei@imb-cnm.csic.es>

[a] Instituto de Microelectrònica de Barcelona IMB-CNM (CSIC), address: Campus UAB, Carrer dels Til·lers, 08193 Cerdanyola del Vallès, Barcelona, Spain

• **Corresponding author.**

Michele Dei <michele.dei@imb-cnm.csic.es>

Abstract

The determination of ethanol intoxication in whole blood samples may open the opportunity for a precise and quick point-of-measurement for action taking in the ambit of medical emergency or law enforcement. In contrast with traditional techniques based on breath sampling, direct blood measurements present greater immunity to errors specially in case of unconscious or non-collaborative patients. In this context, a portable, high-sensitive and user-friendly instrument is highly desirable.

In the current work we present a smartphone-based µPotentiostat which combines a novel circuital technique for sensor readout digitalization. Such system allows both chronoamperometric and cyclic voltammetry measurements with a reduced number of electronic components on a compact PCB (38.5 × 22.5 mm^2). Power, data-link and user interface is provided in combination with a standard smartphone, enabling this cost-effective instrument to have a usability, reconfigurability and an accuracy of the same order of commercial benchtop instruments. The readout platform discussed in this work has been coupled to lab-on-a-chip for point-of.care combining Pt electrodes microfabricated on silicon substrate for electrochemical measurement and a microfluidic structure of methacrylate for fluid management. Biosensing is enabled by in situ electrodeposition of a calcium alginate hydrogel containing horseradish peroxidase (HPR) and alcohol oxidase (AOx) for selective ethanol detection. Alginate membrane

electrodeposition has been here optimized for rapid generation (2 minutes) and to retain the cellular fraction, thus allowing the measurement in while blood samples.

The µPotentiostat features a sensitivity of 37 nA/gL^{-1} to ethanol concentration in blood in the 0-1 gL^{-1} range, with a limit of quantification (LoQ) of 4.5 nA, which is a suitable response for discerning the legal, illegal, severely illegal bounds in a 40 µL sample of blood.

Highlights

• Rapid and precise point-of-measurements of ethanol intoxication in whole blood sample.

• A compact and low-cost smartphone-based µPotentiostat platform bridging from the transducer up to the graphical user interface was devised, showing LoD of 1.35 nA and LoQ 4.5 nA.

• Lab-on-a-chip based on calcium alginate hydrogels for selective determination of ethanol in whole blood samples.

• Ethanol concentration in 40 µL blood sample is sensed in the 0-1 gL^{-1} range with a sensitivity of 37 nA/gL^{-1}.

Keywords

Smartphone-based micro-potentiostat; Low-cost reusable point-of-measurement; Whole blood analysis lab-on-a-chip; Blood-alcohol concentration; Ethanol intoxication.

1. Introduction

The degree of ethanol intoxication of a person is assessed in a number of circumstances including traffic police checkpoints, emergency departments or emergency quick responses (Kaisdotter Andersson et al., 2015; Sebbane et al., 2012) and is quantified by blood alcohol concentration (BAC). Currently, hand-held breath analyzers (commonly referred to braethalyzers) are employed either for law enforcement in traffic security or in clinical trials. These devices sample patients' breath alcohol concentration (BrAC) in a rapid and non-invasive way and rely on an established BrAC/BAC ratio (BBR) to finally estimate patients' BAC. Despite the versatility of these devices, their reliability in critical cases such as emergency situations is undermined by: (i) BBR inter-/intra-individual variability, (ii) respiratory impairment or lack of patient collaboration and (iii) presence of residual mouth alcohol. BBR values vary a lot among different countries, depending on the respective legal framework for traffic security and ranging from a 2000 to 2400 (Logan and Osselton, 2011), giving rise to a fervid scientific debate (Hartung et al., 2016; Jones, 2016; Kriikku et al., 2014). Subject will and/or capacity to sustaining a constant breath flow through the instrument is another issue that can only be addressed by the most sophisticated and expensive models of breathalyzers. Finally test results can be false positive due to the presence of alcohol in the mouth, but not absorbed in the bloodstream: use of mouth rinses or even endogenous fermentation in human guts are possible causes of that (Lindberg et al., 2015). For these reasons, in many countries BrAC are confirmed with a blood analysis in the hospital before taking a decision.

Alternatively, a simple direct BAC measurement on a very small quantity of blood, in the same fashion of common diabetes tests, can overcome all the above mentioned issues. In the era of the maturing Internet of Things, such point-of-care/point-of-measurement instrument should be thought as a low-cost plug-and-play extension to the almost universally diffused smart devices (phones, tablets, convertible laptops). Smartphone-based electrochemical instruments for health monitoring are in vogue among the scientific community in the recent years, promising portable, real-time, cloud-connected and inexpensive measurements capable of basic potentiostatic operation, chronoamperometry (CA), cyclic voltammetry (CV), electrochemical impedance spectroscopy (EIS) (Aggidis et al., 2015; Quesada-González and Merkoçi, 2017; Roda et al., 2016; Zhang and Liu, 2016). Cost is an important parameter of these solutions when penetration in the market is considered in the near future, and it is generally determined by the number of discrete components used to link the transducer electrodes to the computational power of a smartphone: in the current state of the art, the best cost-effective solution is reported in (Wang et al., 2015) (10$) while other solutions score above $20 (Alexander C. Sun, Chengyang Yao, A.G. Venkatesh, 2016; Andres Felipe Diaz Cruz, Nicolas Norena, Ajeet Kaushik, 2014; Carlyn Loncaric, Yiting Tang, Cassie Hob, M. Ash Parameswaran, 2012; Daizong Ji, Lei Liu, Shuang Li, Chen Chen, Yanli Lu, Jiajia Wu, 2017; Eliah Aronoff-Spencer, A.G. Venkatesh, Alex Sun, Howard Brickner, David Looney, 2016; Ioannis Ramfosa, Nikolaos Vassiliadis, Spyridon Blionas, Konstantinos Efstathiou, Alex Fragoso, Ciara K. O'Sullivan, 2013; Lillehoj et al.,

2013; Nemiroski et al., 2014; Rowe et al., 2011; Wang et al., 2017; Yan Fan, Juntao Liu, Yang Wang, Jinping Luo, Huiren Xu, 2017). However the system in (Wang et al., 2015) is based on audio jack connection which, differently from USB connectivity, is not available in most of the last generation smartphones.

Here we present a portable instrument for BAC measurement device employing the recently published transducer structures based on electrodeposited alginate membranes (Márquez et al., 2017) in combination with an original circuit architecture enabling the integration of complex functions over readout signals using very few discrete components. The resulting very low-cost (<10$) and reusable Lab-On-Chip (LOC) allows BAC assessment in whole blood samples which are emergency point-of-measurements, where rapidity, versatility and simplicity are of paramount importance.

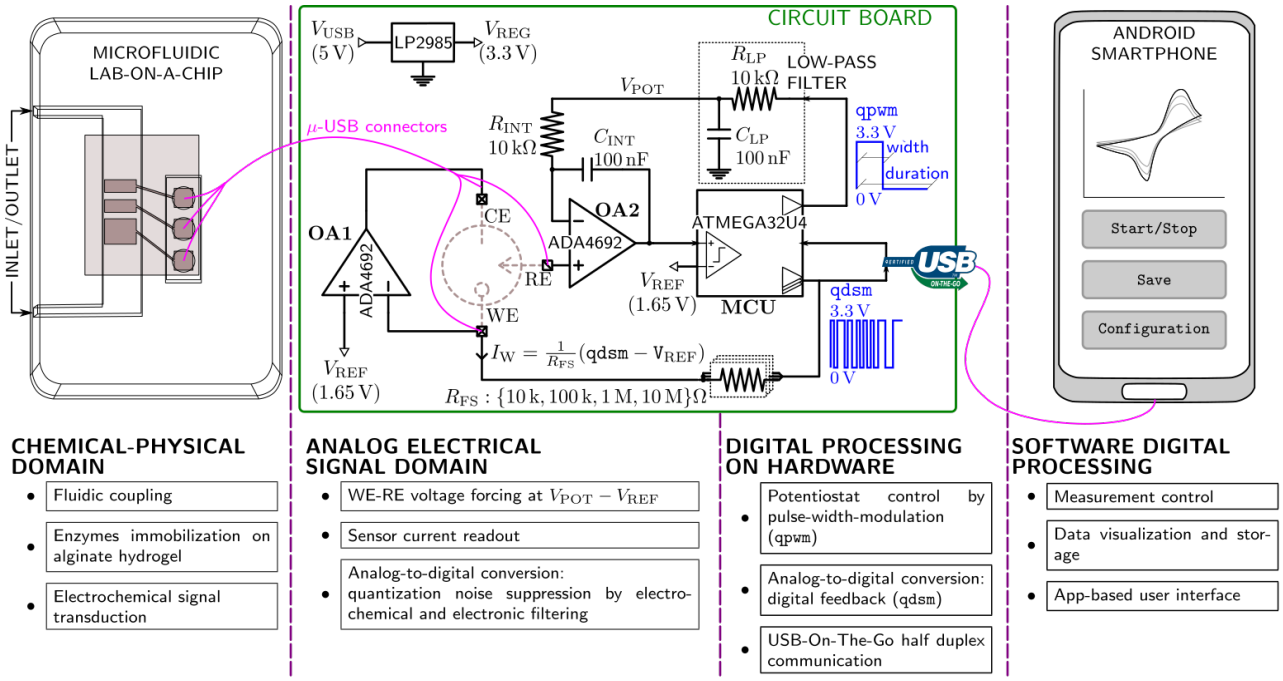

Fig.1. Smartphone-based µPotentiostat for BAC assesment: from sensing to end-user interface.

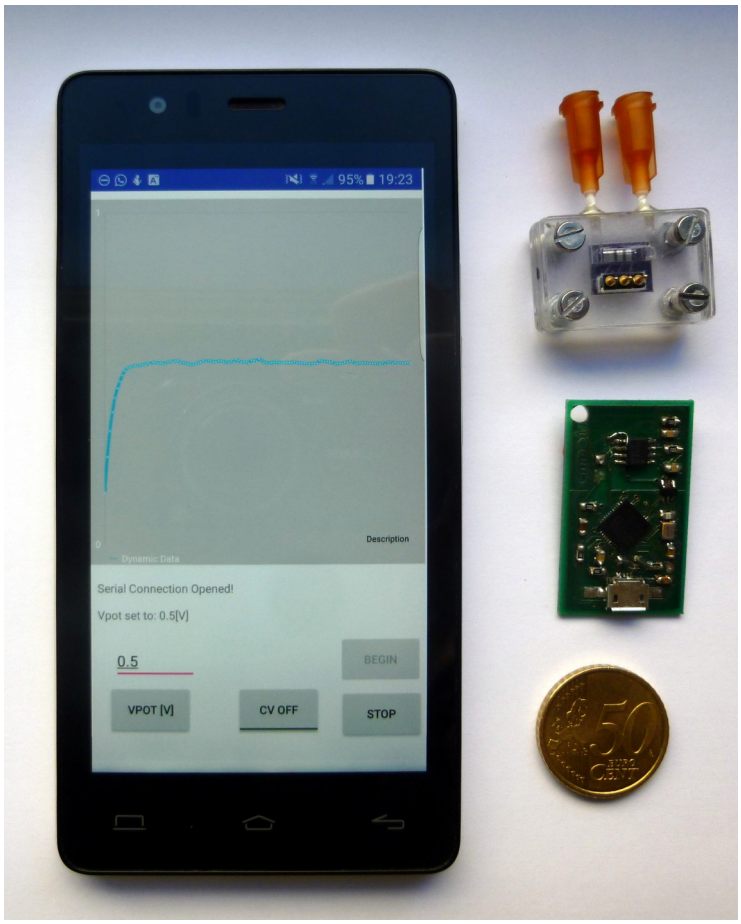

Fig.2. Photograph of the Smarphone-based µPotentiostat.

2. Material and methods

2.1 Architecture of the smartphone-based electrochemical instrument

Figure 1 depicts the system concept and the detailed functions from the electrochemical transduction up to the data capture and visualization on an Android-based smartphone. The extremely compact design of the printed circuit board (PCB) is based on original circuital topologies which reuses the intrinsic electrochemical time constant and a few electrical components to implement a flexible-yet-high resolution potentiostat (Aymerich et al., 2017; Sutula et al., 2014). Such miniaturized USB-powered PCB is capable to operate the sensor in potentiostatic, cyclic voltammetry and chronoamperometry mode. Thus being highly reconfigurable. In this novel architecture, a number of design techniques combining the electrochemical, analog-to-digital conversion and mixed hardware/software aspects concur to drastically reduce the list of components and thus the cost of the final system.

The working electrode voltage is set to 1.65 V, i.e. at half the regulated supply, by the local negative feedback loop built around an operational amplifier (OA1). This feedback loop compensates for the current I_W at the working electrode (WE) counteracting at counter electrode (CE). This condition is reinforced by using ultra-low input currents operational amplifiers (both OA1 and OA2) which avoid parasitic charge flows, especially at the reference electrode (RE).

Another control loop, namely the Delta-Sigma loop, is implemented around the sensor. The feedback loop is closed through OA2, the microcontroller (MCU) and resistor R_{FS}. The main purpose of this loop is to provide the analog-to-digital conversion of the sensor redox current through the output modulated signal *qdsm*. A simple way to describe the Delta-Sigma action is as follows: whenever I_W imbalances the sensor redox current, charge is either accumulated in or depleted from the electrochemical cell. This allows instantaneous small variations of the reference voltage (V_{RE}) with respect to its DC value (V_{POT}), which should be accounted as instantaneous errors. The error is accumulated by the integrator build around OA2 in form of a charge stored in C_{INT}. The voltage output of OA2, holding the information of the error charge, is connected to the MCU comparator input port. Periodically, at a pace provided by the MCU clock, the accumulated error is assessed to be either positive or negative. Consequently, the MCU output digital drivers set the voltage across the R_{FS}, thus the feedback current I_W, to compensate for the accumulated error.

At this point, it is important to notice that the MCU sampling frequency, set to 4 kHz, pushes the error fluctuations far from the sensor intrinsic bandwidth, providing an effective frequency domain decoupling of the control signal with respect to the redox signal. On the other hand, the negative feedback nature of the Delta-Sigma loop forces the DC component of I_W to follow the redox current generated by the sensor. As indicated in Fig. 1, I_W polarity is determined by the signal *qdsm*, which is finally the digital representation of

the redox current and can be readily transmitted through a USB-On-The-Go (USB-OTG) cable to a smartphone for data capture and visualization.

The same loop also provides the correct potentiostatic DC voltage since any difference between V_{POT} and V_{RE} is also accumulated into the electronic integrator and then corrected by the Delta-Sigma loop.

Finally, V_{POT} is generated by low-pass filtering a pulse-width modulated digital signal (*qpwm*) also coming from the MCU. Since the low-pass filter extracts the DC value of *qpwm* by simply modifying the width of the pulses, V_{POT} can span from 3.3 V to 0 V, which corresponds to a potentiostatic setting point between -1.65V and 1.65 V. Different current full-scales (165 nA to 165 µA) are set by parallelizing multiple MCU three-state digital buffers attached to weighted resistors R_{FS}. Both full-scale current and V_{POT} values can be digitally programmed by the MCU accessed by the user through the intuitive user interface implemented on an Android device.

2.2 Electronic components and software programming

Surface Mounted Devices (SMD) 0805 resistors/capacitors, SMD single chip dual operational amplifiers ADA4692-2, voltage regulator LP2985, ATMega32U4 AVR MCU soldered on a standard double layer PCB (size: 38.5 mm × 22.5 mm). The selected MCU has a built-in USB signalling capability which made additional USB chipset unecessary. The micro USB-OTG cable has been obtained from a standard USB cable for smartphones by grounding the fifth pin in the male micro-USB connector.

The Arduino Leonardo firmware has been flashed onto the MCU by using a standard Arduino board as in-system program (ISP), allowing to handle USB connectivity and programming without any external hardware programmer. This allowed to use the user friendly and very popular Arduino development environment.

A very simple android application has been developed in Android Studio 2.3.1. which allows for opening the serial port connection through the USB cable. The application has two operation modes: CA and CV. In the former mode V_{POT} is set, while the latter mode is defined by the scan rate and the peak-to-peak V_{POT} parameters. Full-scale current is chosen for both operations by a drop-down menu to be set between the following values: 165 nA, 1.65 µA, 16.5 µA, 165 µA. The user starts data acquisition which is recollected in the smartphone memory and visualized by a minimal plot interface. When operated in CV mode, scan-rates can be set between 1 and 200 mV/s.

2.3 Chemicals and reagents

Alginic acid sodium salt, $CaCl_2$ (≥93 %), 2-(N-morpholino)ethanesulfonic acid hydrate (MES hydrate, ≥99 %), NaOH (≥98 %), KOH (≥86 %), 3,3′,5,5′-Tetramethylbenzidine (TMB, ≥98 %), NaCl (ACS reagent, ≥99 %), H_2O_2 (30% in H_2O), HRP (Type VI-A, essentially salt-free lyophilized powder, 250-330 units mg^{-1}) and AOx from *Pichia pastoris* (buffered aqueous solution, 1200 units ml^{-1}) were purchased from Sigma-Aldrich. $CaCO_3$ (≥98.5 %), $K_3[Fe(CN)_6]$ (ACS reagent, ≥99 %), dimethyl sulphoxide (DMSO, 99.5 %), Na_2HPO_4 (ACS reagent,

≥99 %) and ethanol absolute (≥99.5 %) were purchased from Panreac. KCl (≥99 %) and KH_2PO4 (ACS reagent, ≥99.5 %) were purchased from Fluka.

All chemicals were used as received and aqueous solutions were prepared using de-ionized water with a resistivity of 2 M Ω cm. Used PBS contains NaCl (8 g L^{-1}), KCl (0.2 g L^{-1}), Na_2HPO_4 (1.42 g L^{-1}) and KH_2PO_4 (0.24 g L^{-1}). TMB 50 mM stock solution was daily prepared using DMSO as solvent. Whole blood was extracted from a volunteer and stored at 4° C until measurement.

2.5 Equipment

For electrical and electrochemical characterization of the home-made µPotentiostat, a µAutolab potentiostat Type-III containing the FRA32 module for electrochemical impedance spectroscopy analysis and controlled with Nova 2.0 software was used. The pH of the used buffer was established using a Crison pH & ION-Meter GLP 22+.

2.6 Electrochemical transducer

For the electrochemical part of the biosensor, a three Pt electrodes linear array was used as pseudo-reference, working and counter electrodes respectively. The electrodes set was fabricated on a silicon substrate at the IMB-CNM clean room facilities, according to a previously described photolithographic process (Orozco et al., 2007).

The presented electrodes do not precise of electrical bonding as they are linked to adjacent areas of the same material, later coupled by spring loaded connectors to the µPotentiostat.

2.7 Microfluidic LOC

A PMMA-PDMS structure was designed and fabricated in accordance with the silicon substrate. The PMMA and PDMS pieces were designed using CorelDRAW V7 software and then cut with an Epilog Mini 24 CO_2 laser ablation machine. The LOC structure was designed and constructed layer by layer in three blocks: i) a base adapted to the Si substrate fingerprint for the stable positioning of the chip, ii) the microfluidic layer, containing the microchannels for liquid managing and the measurement and iii) a cover layer to seal the system. The different PMMA pieces were joined using a pressure-sensitive adhesive (PSA) for the definitive unions while the PDMS layers where used as sealing ring between blocks to facilitate the disassemble of the device. Four screws in the corners of the device prevents any leakage between the PMMA and PDMS layers. The inlet and outlet of the channel were glued to a conventional fluidic connector using epoxy resin. Prior to use, the electrodes were cleaned by immersion during 10 min in an aqueous solution containing 0.05 M KOH and 25 % w/v H_2O_2.

2.8 Alginate-based biosensor

As the recognition part of the biosensor, a reversible electrodepositable calcium alginate hydrogel was used for the enzymes immobilization, following a previously reported protocol (Márquez et al., 2017). The

measure cycle consists of three main steps: hydrogel electrodeposition, amperometric detection and hydrogel removal, thus being able to use the same electrochemical transducer many times just but in situ regeneration of the biocatalytic membrane. Briefly, for the electrodeposition, an alginic acid sodium salt was dissolved in warm water with magnetic stirring and then mixed with $CaCO_3$ and the enzymes. Subsequently, it was injected into the reaction chamber of the device through the microchannels. In presence of $CaCO_3$ particles, the application of an anodizing potential (1.5 V vs. RE) promotes water oxidation into O_2 and protons. These protons react with the $CaCO_3$ particles, promoting their dissociation into Ca^{2+} cations and HCO_3^-. Finally, the Ca^{2+} cations complete the cross-link reaction among the alginic acid monomers and a gel is formed, attached to the anodized electrode (WE). After the electrodeposition, the chamber is washed with deionized water to remove the excess of precursor and leave only the recently built hydrogel. For the measurement, the sample and the mediator (TMB) were introduced in the chamber and a constant potential of 0 V (vs. Pt RE) was applied between the WE and the RE, while the current was measured between the WE and the CE. The registered current corresponding to the reduction of TMB is related to the initial amount of ethanol in the medium due to the following cascade reaction:

$$CH_3CH_2O + O_2 \xrightarrow{\text{Alcohol Oxidase}} CH_3CHO + H_2O_2 \quad (1)$$

$$H_2O_2 + TMB_{red} \xrightarrow{\text{Horseradish Peroxidase}} H_2O + TMB_{ox} \quad (2)$$

Where the ethanol is first oxidized by the AOx into acetaldehyde and hydrogen peroxide (1) and this is used by the HRP to oxide the TMB (2) which is present as a mediator. Finally, the oxidized TMB is reduced at the WE at the applied potential. Once the measurement is finished, the microfluidic system is flushed with PBS or the removal of the biocatalytic membrane. Concretely, the phosphate acts as a chelating agent, trapping Ca^{2+} and disaggregating the gel rapidly. The process can then start from the beginning in a second analysis using the same device and only regenerating the membrane.

3. Results

3.1 Electrical tests

Since the proposed µPotentiostat follows the idea of (Sutula et al., 2014), where the intrinsic sensor time constant participates in the readout process of the transducer current, electrical characterization of the sensor, in the sense of Randles model, is fundamental. To this purpose experimental impedance measurements of the structures of Section 2.6, have been performed using Autolab. For the circuit model in Fig 2(a), the following electrical parameters have been extracted after fitting: R_S = 52±2 ohm, C_{DL} = 1.392±0.002 µF, R_{CT} = 58±2 kohm, W = 3±2 kohm.

Starting from these values a discrete component RC network, first order matched to the Randles model (Fig. 3(a)), has been assembled in order to emulate the sensor behavior and test the µPotentiostat correct operation (R_S = 330 ohm, C_{DL} = 1.5 µF, R_{CT} = 56 kohm, W = 0). In this first approach the Warburg element has been neglected since its effects are evident only at extremely low frequencies. With such dummy sensor a zero input signal condition can be easily implemented at electrical level which is useful to estimate the instrumentation noise floor. Data acquisition of the *qdsm* signal has been performed in this condition and the resulting power spectrum is shown in Fig. 3(b). As expected, two regions are clearly visible: thermal flat noise dominates up to approximately 80 Hz, while for the higher frequencies the noise profile is dominated by the typical shaped quantization noise due to the Delta-Sigma modulation. The sensor intrinsic bandwidth can be roughly estimated as $1/(2\pi\ R_{CT}\ C_{DL})$ approximately 1.9 Hz. Considering an observation time of 10 seconds, and a bandwidth of 2 Hz, the residual integrated noise is less than 1 nA root-mean-squared (RMS). It is worth noting that the part of the spectrum exceeding the sensor bandwidth will be numerically filtered out by software in the smartphone application.

To further characterize the µPotentiostat, the sensing structures described in Section 2.6 have been submerged in KCl saline solution and have been connected to the PCB to perform chronoamperometric readouts which allowed to determine the limit of detection (LoD) and limit of quantification (LoQ) of 1.35 nA and 4.50 nA, respectively. Systematic current offset due to deviation of the reference voltage from the nominal value of 1.65 V was measured to be 3.84 nA. The testbench described in Section 2.5 returned similar values (LoD = 2.8 nA and LoQ = 9.4 nA), while having negligible current offset. Estimation of LoD and LoQ in has been done considering the 3 and 10 standard deviations, respectively.

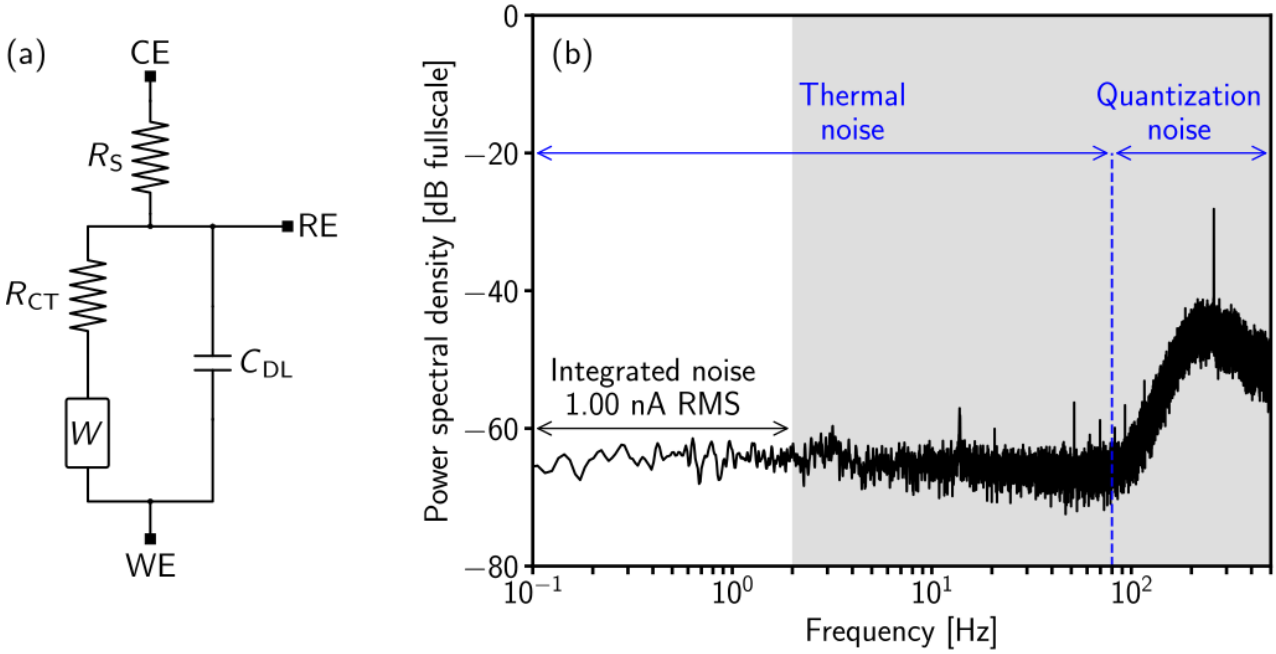

Fig.3. Simplified Randles electrical equivalent circuit (a) and measured electronic readout noise (b).

3.2 Electrochemical test

The µPotentiostat has been characterized through cyclic voltammetry experiments of the $Fe^{III}(CN)_6^{3-}/Fe^{II}(CN)_64^-$ couple. Figure 4 shows the results for a 1 mM Ferri-Ferro in 150 mM KCl at different scan rates compared to the benchtop instrument. For this experiment the R_{FS} was fixed to be 330 kohm, in order to provide a nominal current full-scale of 5 µA (both positive and negative). Data was extracted recording the digital signal *qdsm* sampled at 2.5 kS/s. At this point, since *qdsm* contains the high frequency quantization noise, filtering is needed to correctly reconstruct the WE current waveform. Ideally, an analog Bessel filter should be employed to preserve the group delay of the signal. In practice a digital equivalent derived from the analog model through a bilinear transform is sufficient since the bandwidth of interest is much lower than the sampling frequency. This way the high frequency noise evident in Fig.2 is largely suppressed. The tuning parameter of the filter must be adjusted to accordingly since the bandwidth of interest scales proportionally to the scan-rate. It is worth noting that an excessive filtering should be carefully chosen in order to avoid filtering frequency component of the signal of interest. For the third-order digital Bessel filter used here, the critical frequency at phase response midpoint has been set to 0.67 Hz, 8.33 Hz, 20.83 Hz for the scan-rates of 2 mV/s, 10 mV/s and 25 mV/s, respectively. The comparison between the µPotentiostat versus the bench-top cyclic voltammetries are evident in Fig.4(a) and (b), where it can be seen that some high frequency noise is still visible in out system. A smoother characteristic can be obtained, without bandwidth impairment, by averaging several cycles.

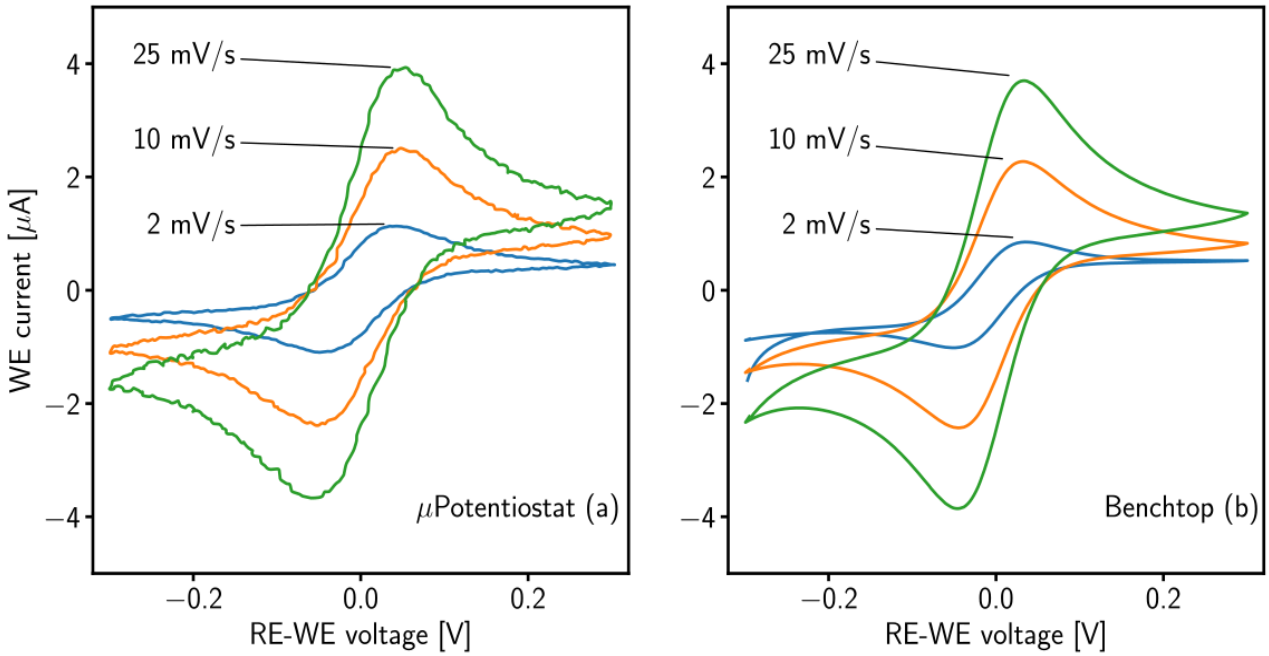

Fig.4. Cyclic voltammetries of 1 mM Ferri-Ferro in 150 mM KCl at different scan rates: (a) µPotentiostat and (b) bench-top setup described in Section 2.5.

3.3 Alcohol biosensor characterization

The biosensor was optimized in order to obtain a fast response time (2 min after analyte addition), a good sensitivity (−54 nA / g L^{-1}) and an accurate linear range for measure (0 to 1 g L^{-1}). For that purpose, the amounts in the precursor of alginic acid (1% w/v), $CaCO_3$ (0.5 % w/v) and HRP (25 units ml^{-1}) were fixed while the amount of AOx was changed from 0.1 to 0.6 units ml^{-1}, reaching the saturation response of the biosensor in buffer at 0.4 units ml^{-1} (Fig. 5(a)) for the maximum ethanol concentration (1 g L^{-1}). This AOx concentration was considered optimal and used in further experiments. For higher concentration (> 0.5 units ml^{-1}), the response saturates as a consequence of HPR inhibition by an excess of H_2O_2. Moreover, in this region the error bars are larger probably due to appearance of AOx aggregates having a not well controlled orientation of the active sites. For this reason, the value 0.4 units ml^{-1} was selected ensuring at the same time both a good sensitivity and reproducibility.

Maintaining these conditions for the membrane electrodeposition, the biosensor was calibrated using buffer solutions with different ethanol concentrations, from 0.25 to 1 g L^{-1}. The buffer solution contained 0.2 M MES-NaOH pH 7, 0.145 M KCl, 0.01 M $CaCl_2$ and 1.5 mM TMB.

The different solutions were injected in the cell through the microchannel and then a chronoamperometric measurement was started applying a constant potential of 0 V vs Pt. (RE). Figure 5(b) reports the linear range of the calibration curve when plotting the current sampled at 60 seconds after the potential application as function of ethanol concentration. Each point in the calibration curve corresponded to the

measurement of an independent membrane. The small variation between points demonstrated the repeatability of the electrodeposition process and the quality, stability and durability of the microelectrodes used in this work, something impossible to attain with low-cost screen printed electrodes.

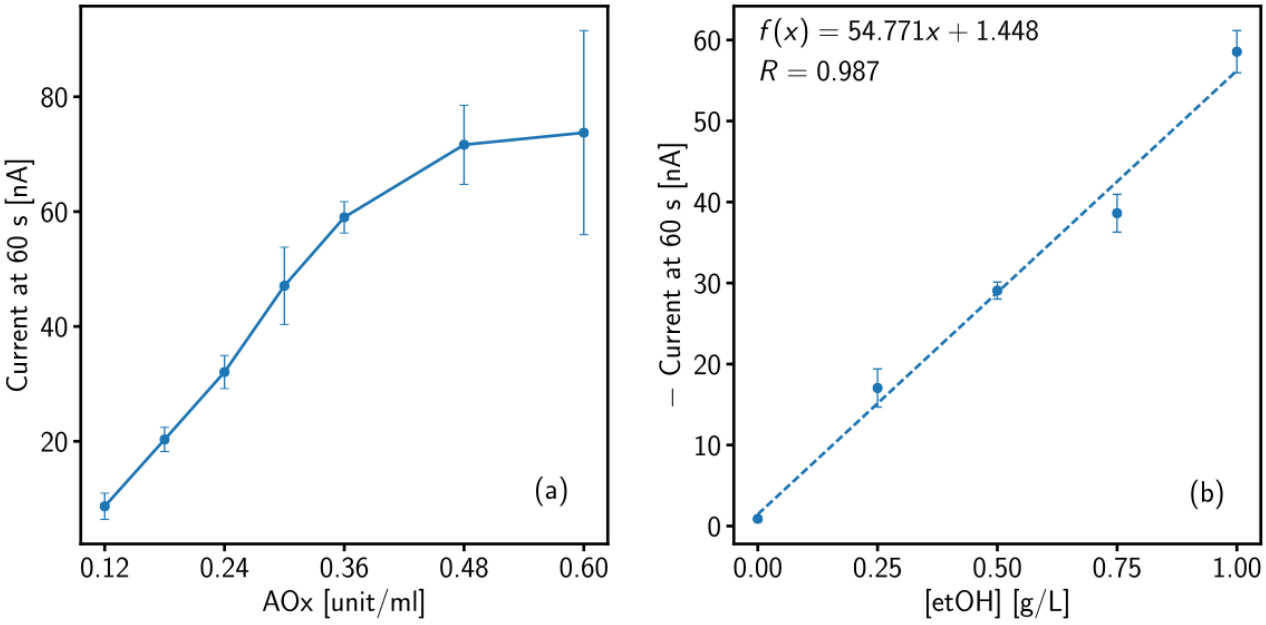

Fig.5. AOx quantification for optimized etOH sensing (a) and sensor calibration in buffer solution (b): 0.2 M MES-NaOH pH 7, 0.145 M KCl, 0.01 M $CaCl_2$ and 1.5 10^{-3} M TMB.

3.4 Alcohol determination in whole blood samples

In the case of real samples, 40 µL of whole blood were mixed with 2 µL of 50 mM TMB and 8 µL of aqueous ethanol solutions at different concentrations yielding to different final ethanol concentrations. In this case, the sample is not injected through the microchannel because of its small volume. Therefore, the cover piece is modified with a cavity situated over the WE that can be open for the blood addition. Due to diffusion limitations, 2 minutes were stablished as incubation time prior to measurement to ensure the stability of the recorded signal. The use of alginate in case of complex samples analysis such as whole blood is essential in order to protect the WE from biofouling and obtain a good response as it has been reported previously (Márquez et al., 2017).

Figure 6 illustrate the sensor current response within the 0–1 g L^{-1} range. The resulting calibration curve of Fig. 5(b) shows a good correlation between the registered current and the amount of ethanol added to the blood samples, although there is a loss of sensitivity compared to buffer calibrations probably due to matrix effects. Nonetheless, the current low-cost and portable smartphone-based platform merging a minimalistic and reconfigurable µPotentiostat with a durable amperometric Lab-on-a-Chip architecture enables the accurate and fast in-situ determination of ethanol concentration in whole blood samples.

The precision of the µPotentiostat can be estimated by inverting the linear regression curve reported in Fig. 6 and projecting the current readout uncertainty on the measurand. Applying this procedure, a maximum error of 0.084 g L^{-1} has been found in the 0 – 0.5 g L^{-1} range.

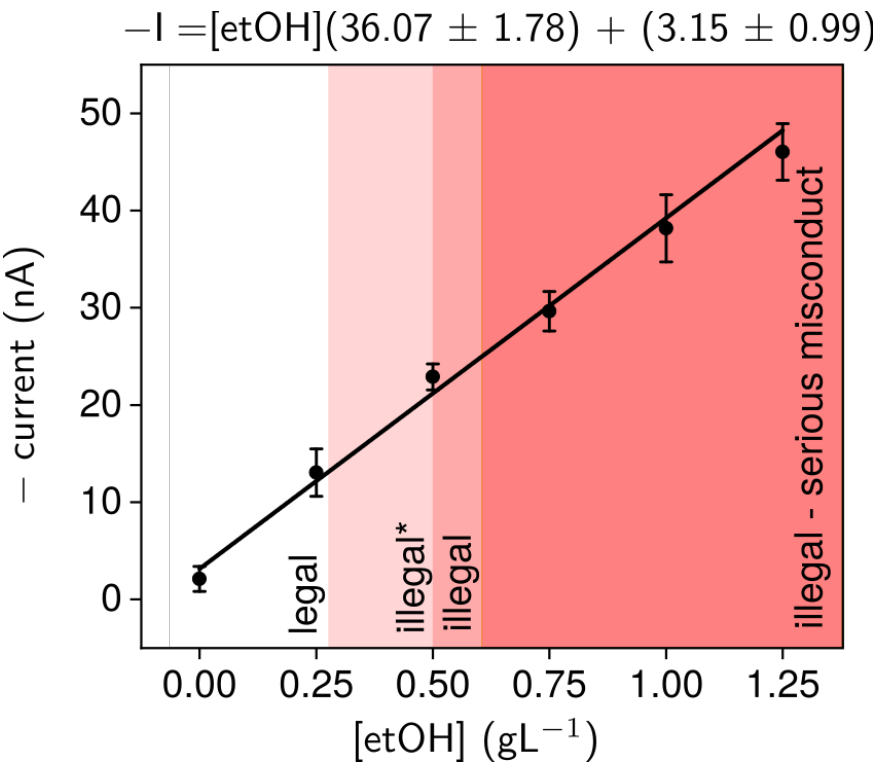

Fig.6. Whole blood measurement spiked with etOH. Legal limits according to Spanish traffic code. Illegal* for novice and professional drivers.

4. Conclusions

In conclusion, blood alcohol rate determination in whole blood samples is possible with the portable, miniaturized and lightweight smartphone-based LoC presented in the current study. The system inherently performs the potentiostatic amperometric readout of the sensor current through an electrochemical feedback loop providing a Delta-Sigma modulated digital stream which is conveniently processed using the signal processing resources of standard Android smartphone, without the need of dedicated digital processing hardware. This novel readout technique proved to be reconfigurable, it operates cyclic voltammetries and chronoamperometric measurements with LoD and LoQ comparable with commercial benchtop instruments. The use of the smartphone, moreover, offers a simple graphical interface and opens the possibility to benefit from cloud-based services for data flow under the Internet-of-things scenario. The ethanol transducing element is an alginate-based biosensor specifically optimized for accurate and linear response in the 0–1 g L^{-1} range, which is of interest for action taking both from medical and law enforcement point of view.

High-precision breath-testing machines such as BAC DataMaster, currently used as evidential instrument in many countries, is guaranteed to have a margin of error confined between 0.001 % w/v and 0.003 % w/v. In this respect, our solution showed an estimated error lower than 0.009 % w/v considering the worst case error in the 0 – 0.5 g L^{-1} range. The precision of the proposed LoC, despite its low-cost concept, is comparable with much more sophisticated, bulky and expensive instruments.

Authors, with the aim to contribute to the development of advanced LoC for emergency point-of-measurements, are currently developing a custom integrated circuit implementation of the readout interface here presented, which is envisioned to greatly improve the sensibility, integrability and cost effectiveness of the system.

Acknowledgements

The research leading to these results has received funding from the People Programme (Marie Curie Actions) of the Seventh Framework Programme of the European Union (FP7/2007-2013) under REA grant agreement no. 600388 (TECNIOspring programme: TECSPR16-1-0056), and from the Agency for Business Competitiveness of the Government of Catalonia, ACCIÓ. This work was partially supported by the Spanish R & D Noational Program (MEC Project TEC2014-5449-C3-1-R). Dr. X. M.-B. also acknowledge the “Ramón y Cajal” program from the Spanish Government. A.M. is also grateful to the MICINN for the award of a studentship from FPI program (BES-2015-072946).

References

Aggidis, A.G.A., Newman, J.D., Aggidis, G.A., 2015. Investigating pipeline and state of the art blood glucose biosensors to formulate next steps. Biosens. Bioelectron. 74, 243–262. https://doi.org/http://dx.doi.org/10.1016/j.bios.2015.05.071

Alexander C. Sun, Chengyang Yao, A.G. Venkatesh, D.A.H., 2016. An efficient power harvesting mobile phone-based electrochemical biosensor for point-of-care health monitoring. Sensors Actuators B Chem. 235, 126–135. https://doi.org/10.1016/J.SNB.2016.05.010

Andres Felipe Diaz Cruz, Nicolas Norena, Ajeet Kaushik, S.B., 2014. A low-cost miniaturized potentiostat for point-of-care diagnosis. Biosens. Bioelectron. 62, 249–254. https://doi.org/10.1016/J.BIOS.2014.06.053

Aymerich, J., Dei, M., Terés, L., Serra-Graells, F., 2017. Design of a low-power potentiostatic second-order CT Delta-Sigma ADC for electrochemical sensors, in: 2017 13th Conference on Ph.D. Research in Microelectronics and Electronics (PRIME). pp. 105–108. https://doi.org/10.1109/PRIME.2017.7974118

Carlyn Loncaric, Yiting Tang, Cassie Hob, M. Ash Parameswaran, H.-Z.Y., 2012. A USB-based electrochemical biosensor prototype for point-of-care diagnosis. Sensors Actuators B Chem. 161, 908–913. https://doi.org/10.1016/J.SNB.2011.11.061

Daizong Ji, Lei Liu, Shuang Li, Chen Chen, Yanli Lu, Jiajia Wu, Q.L., 2017. Smartphone-based cyclic voltammetry system with graphene modified screen printed electrodes for glucose detection. Biosens. Bioelectron. 98, 449–456. https://doi.org/10.1016/J.BIOS.2017.07.027

Eliah Aronoff-Spencer, A.G. Venkatesh, Alex Sun, Howard Brickner, David Looney, D.A.H., 2016. Detection of Hepatitis C core antibody by dual-affinity yeast chimera and smartphone-based electrochemical sensing. Biosens. Bioelectron. 86, 690–696. https://doi.org/10.1016/J.BIOS.2016.07.023

Hartung, B., Ritz-Timme, S., Daldrup, T., 2016. Advantages and disadvantages of breath alcohol analysis-Reply to “Evidential breath alcohol analysis and the venous blood-to-breath ratio.” Forensic Sci. Int. https://doi.org/10.1016/j.forsciint.2016.03.011

Ioannis Ramfosa, Nikolaos Vassiliadis, Spyridon Blionas, Konstantinos Efstathiou, Alex Fragoso, Ciara K. O’Sullivan, A.B., 2013. A compact hybrid-multiplexed potentiostat for real-time electrochemical biosensing applications. Biosens. Bioelectron. 47, 482–489. https://doi.org/10.1016/J.BIOS.2013.03.068

Jones, A.W., 2016. Evidential breath alcohol analysis and the venous blood-to-breath ratio. Forensic Sci. Int. https://doi.org/10.1016/j.forsciint.2016.03.008

Kaisdotter Andersson, A., Kron, J., Castren, M., Muntlin Athlin, A., Hok, B., Wiklund, L., 2015. Assessment of the breath alcohol concentration in emergency care patients with different level of consciousness. Scand. J. Trauma. Resusc. Emerg. Med. https://doi.org/10.1186/s13049-014-0082-y

Kriikku, P., Wilhelm, L., Jenckel, S., Rintatalo, J., Hurme, J., Kramer, J., Wayne Jones, A., Ojanperä, I., 2014. Comparison of breath-alcohol screening test results with venous blood alcohol concentration in suspected drunken drivers. Forensic Sci. Int. https://doi.org/10.1016/j.forsciint.2014.03.019

Lillehoj, P.B., Huang, M.-C., Truong, N., Ho, C.-M., 2013. Rapid electrochemical detection on a mobile phone. Lab Chip 13, 2950–2955. https://doi.org/10.1039/c3lc50306b

Lindberg, L., Grubb, D., Dencker, D., Finnhult, M., Olsson, S.G., 2015. Detection of mouth alcohol during breath alcohol analysis. Forensic Sci. Int. https://doi.org/10.1016/j.forsciint.2015.01.017

Logan, B.K., Osselton, M.D., 2011. Driving under the influence of drugs, in: Clarke's Analysis of Drugs and Poisons : In Pharmaceuticals, Body Fluids and Postmortem Material.

Márquez, A., Jiménez-Jorquera, C., Domínguez, C., Muñoz-Berbel, X., 2017. Electrodepositable alginate membranes for enzymatic sensors: An amperometric glucose biosensor for whole blood analysis. Biosens. Bioelectron. 97, 136–142. https://doi.org/10.1016/J.BIOS.2017.05.051

Nemiroski, A., Christodouleas, D.C., Hennek, J.W., Kumar, A.A., Maxwell, E.J., Fernández-Abedul, M.T., Whitesides, G.M., 2014. Universal mobile electrochemical detector designed for use in resource-limited applications. Proc. Natl. Acad. Sci. U. S. A. 111, 11984–9. https://doi.org/10.1073/pnas.1405679111

Orozco, J., Suárez, G., Fernández-Sánchez, C., McNeil, C., Jiménez-Jorquera, C., 2007. Characterization of ultramicroelectrode arrays combining electrochemical techniques and optical microscopy imaging. Electrochim. Acta 53, 729–736. https://doi.org/10.1016/J.ELECTACTA.2007.07.049

Quesada-González, D., Merkoçi, A., 2017. Mobile phone-based biosensing: An emerging "diagnostic and communication" technology. Biosens. Bioelectron. 92, 549–562. https://doi.org/10.1016/J.BIOS.2016.10.062

Roda, A., Michelini, E., Zangheri, M., Fusco, M. Di, Calabria, D., Simoni, P., 2016. Smartphone-based biosensors: A critical review and perspectives. TrAC Trends Anal. Chem. 79, 317–325. https://doi.org/http://dx.doi.org/10.1016/j.trac.2015.10.019

Rowe, A.A., Bonham, A.J., White, R.J., Zimmer, M.P., Yadgar, R.J., Hobza, T.M., Honea, J.W., Ben-Yaacov, I., Plaxco, K.W., 2011. CheapStat: An Open-Source, "Do-It-Yourself" Potentiostat for Analytical and Educational Applications. PLoS One 6, e23783. https://doi.org/10.1371/journal.pone.0023783

Sebbane, M., Claret, P.G., Jreige, R., Dumont, R., Lefebvre, S., Rubenovitch, J., Mercier, G., Eledjam, J.J., De La Coussaye, J.E., 2012. Breath analyzer screening of emergency department patients suspected of alcohol intoxication. J. Emerg. Med. https://doi.org/10.1016/j.jemermed.2011.06.147

Sutula, S., Cuxart, J.P., Gonzalo-Ruiz, J., Muñoz-Pascual, F.X., Terés, L., Serra-Graells, F., 2014. A 25-µW All-MOS Potentiostatic Delta-Sigma ADC for Smart Electrochemical Sensors. IEEE Trans. Circuits Syst. I Regul. Pap. 61, 671–679. https://doi.org/10.1109/TCSI.2013.2284179

Wang, X., Gartia, M.R., Jiang, J., Chang, T.-W., Qian, J., Liu, Y., Liu, X., Liu, G.L., 2015. Audio jack based miniaturized mobile phone electrochemical sensing platform. Sensors Actuators B Chem. 209, 677–685. https://doi.org/10.1016/j.snb.2014.12.017

Wang, X., Lin, G., Cui, G., Zhou, X., Liu, G.L., 2017. White blood cell counting on smartphone paper electrochemical sensor. Biosens. Bioelectron. 90, 549–557. https://doi.org/10.1016/j.bios.2016.10.017

Yan Fan, Juntao Liu, Yang Wang, Jinping Luo, Huiren Xu, S.X.X.C., 2017. A wireless point-of-care testing system for the detection of neuron-specific enolase with microfluidic paper-based analytical devices. Biosens. Bioelectron. 95, 60–66. https://doi.org/10.1016/J.BIOS.2017.04.003

Zhang, D., Liu, Q., 2016. Biosensors and bioelectronics on smartphone for portable biochemical detection. Biosens. Bioelectron. 75, 273–284. https://doi.org/http://dx.doi.org/10.1016/j.bios.2015.08.037